2017 International Symposium on Nonlinear Theory and Its Applications,
NOLTA2017, Cancun, Mexico, December 4-7, 2017

Single-Electron Decoder Circuits for Communication Systems Using Photoelectric Effect and Electron Wave Frequency Discrimination

Jinya Sato†, Shota Hayakawa†, Atsushi Setsuie†, Hisato Fujisaka†, and Takeshi Kamio†

†Faculty of Information Science, Hiroshima City University, 731-3194 Japan
Email: hayakawa@sp.info.hiroshima-cu.ac.jp

Abstract—Applications of quantum mechanical phenomena to front-end parts in receivers of Tera-hertz (THz) sensing and communication systems have been studied for minitualization and low-power consumption. THz-detection by photoelectric effect and frequency discrimination by electron-wave coupling and refraction are the examples of the studies. The studies are the attempts to classify photoelectrons by their momentum depending on the frequency of the received THz wave. If the time sequence of the classification represents transmitted data and a decoder circuit analyzing the sequence can be developed, communication equipped with error correction is attained. In this report, such decoder circuits are designed with single-electron tunneling junctions which are suitable to deal with photoelectrons. In addition, circuit simulation presents that the designed decoders function as intended.

1. Introduction

In recent years, sensing and communication systems using Tera-hertz (THz) frequency band have been studied for safety nondestructive sensing and high-speed and high-directional short range communication [1]. Front-end circuits for the receivers of the systems have been developed by extending conventional electronic circuits processing millimeter waves based on classical electromagnetics.

On the other hand, studies on front-end circuits exploiting quantum mechanics have just started [2, 3, 4, 5]. Although there exist many difficulties to be overcome, the researches are useful for minitualization and low-power consumption of the systems. THz-detection by photoelectric effect and frequency discrimination by electron-wave coupling and refraction are the examples of the studies. The studies are the attempts to classify photoelectrons by their momentum depending on the frequency of the received THz wave. If the time sequence of the classification represents transmitted data and a decoder circuit analyzing the sequence can be developed, communication equipped with error correction is attained.

In this report, such decoder circuits are designed with single-electron tunneling (SET) junctions [6] which are suitable to deal with photoelectrons directly. In addition, circuit simulation is carried out to validate that the designed decoders function as intended.

Most parts of this paper were presented in [7] in Japanese.

2. Architecture of the Communication Systems

Figure 1 shows a conceptual framework of the communication system [4, 5]. The system employs a multi-level frequency shift keying as a modulation scheme.

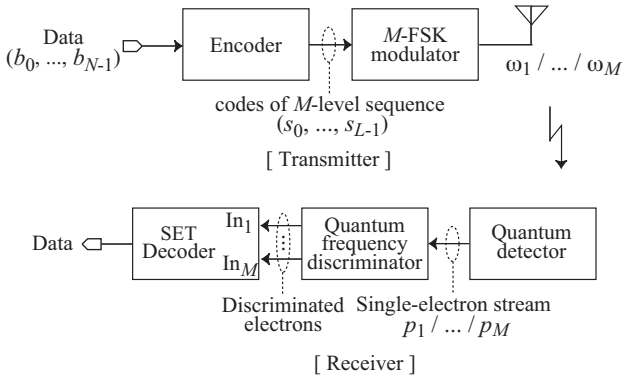

Figure 1: A communication system based on quantum mechanics.

The upper part shows a transmitter. In the transmitter, N-bit data $(b_0, \cdots, b_{N-1})$, $b_n \in \{0, 1\}$, $n = 0, \cdots, N-1$, is mapped into a code of a set of 2^N codes with length L. We denote the code by $S^j = (s_0^j, \cdots, s_{L-1}^j)$, $j = 0, \cdots, 2^N - 1$. The element of the code is an integer of a set of M integers, $s_k^j \in \{\pm 1, \cdots, \pm M/2\}$. Correspondingly, THz-wave of frequency $\omega_k^j \in \{\omega_1, \cdots, \omega_M\}$ is outputted from the transmitter.

The lower part of Fig. 1 is a receiver based on quantum mechanics. Receiving the THz-wave of frequency ω_m, the detector outputs a photoelectron with kinetic energy in proportion to the photon energy of the wave, $p_m^2/m_e \propto \hbar\omega_m$, $m = 1, \cdots, M$, p_m: momentum, m_e: electron mass, $\hbar$: Planck constant divided by 2π. When $M = 2$, a frequency discriminator which consists of coupled electron-wave guides separates the photoelectrons into two groups based on their momentum p_1, p_2 [3, 4]. When $M \geq 3$, a frequency discriminator which is an electron-wave lens classifies the photoelectrons into M groups depending on their momentum p_m [2, 5]. Classified photoelectrons enter into one of the M inputs of the SET decoder. The decoder estimates transmitted data from the input sequence.

3. Decoder Circuit

3.1. Circuit Elements

We explain briefly SET circuit elements used in the decoder.

Figure 2 shows an interface circuit between the discriminator and the decoder. A photoelectron outputted from the discriminator is trapped in an input capacitor of a NOT gate, that is, the capacitor is charged with the electron. Before the next photoelectron comes, clock signal ϕ is given and the single-electron charge

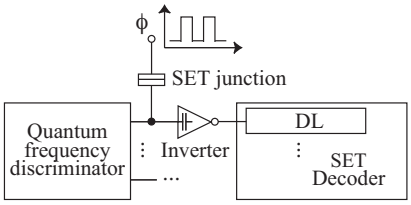

Figure 2: Interface circuit between the frequency discremenator and the decoder.

in the capacitor is discharged through an SET junction.

Unit-delay circuits presented in [8] are adopted for the elements of the decoder. Connecting the unit-delay circuits in series, a shift register (DL) is built.

Linear threshold gate (LTG) presented in [9] are employed for the decoder elements. It computes the inner product between input set $(s_0^j, \cdots, s_{L-1}^j)$ and a weight set $(w_0, \cdots, w_{L-1})$. If the inner product is larger than a threshold value ψ, the output of the LTG becomes high. The weight set is determined by the input capacitances.

NOT gates presented in [10] are used in the decoder as buffer circuits.

3.2. Decoder Circuit

We show SET decoders built of DLs and LTGs for the codes of $N = 1$, $M = 2$, and $L = 5$ in Fig. 3(a) and for the codes of $N = 2$, $M = 4$, and $L = 4$ in Fig. 3(b). The decoders have M DLs and the LTGs have ML inputs. NOT gates used as buffer circuits are not shown in the figure.

Input In_m receives photoelectrons with momentum p_m from the frequency discriminator on the preceding stage. DL_m in the decoder is connected to In_m. After receiving a code $C = (c_0, \cdots, c_{L-1})$, unit-delays of DLs hold "1"(an electron) or "0"(nothing) depending on the inputted sequences of photoelectrons. If the k-th unit-delay of DL_m takes 1, received code elements are judged as $c_k = -M/2 + m - 1$ $(1 \le m \le M/2)$ or $c_k = -M/2 + m$ $(M/2 < m \le M)$, $k = 0, \cdots, L-1$. All the outputs of the unit-delays of each DL_m are connected to the inputs of LTGs.

LTG^j of 2^N LTGs with ML inputs computes the correlation (inner product) between the received code C and S^j, $j = 0, \cdots, 2^N - 1$, and compares the computed result with threshold value ψ. In order to compute the correlation given by $R = \sum_k c_k s_k^j$, the LTG input connected to the k-th unit-delay of DL_m is weighted by $w_{\mathrm{in}} \propto |c_k s_k^j|$. Depending on the sign of $c_k s_k^j$, the unit delay is connected to the upper or lower half of the inputs of LTG^j. When R is larger than ψ, the outout level of LTG^j becomes high, which indicates that the received code is $C = S^j$. Whe $N = 1$, only one LTG is used as in Fig. 3(a). The hight/low output level of the LTG indicates that the received code is S^0/S^1 and the transmitted bit is 0/1.

Examples of codes S^j of $N = 1$, $M = 2$, and $L = 5$ are shown in Tab. 1(a). The contents of two DLs are given in Fig. 4(a) when $C = S^0$ is received. Codes S^j of $N = 2$, $M = 4$, and $L = 4$ and their cross-correlation are exemplified in Tab. 1(b). The contents of DLs are shown in Fig. 4(b) when $C = S^0$ is received.

Table 1: Codes S^j and the cross-correlation between them.

(a) N=1, M=2, L=5

Data	Code Sequence S^j
0	S^0 = (+1,+1,-1,+1,-1)
1	S^1 = (-1,-1,+1,-1,+1)

(b) N=2, M=4, L=4

Data	Code Sequence S^j	Correlation S^0	S^1	S^2	S^3
00	S^0 = (+1,-1,+2,-2)	1	3/10	0	-1/10
01	S^1 = (-2,+1,+2,-1)	--	1	-9/10	0
10	S^2 = (+2,-2,-1,+1)	--	--	1	3/10
11	S^3 = (-1,-2,+1,+2)	--	--	--	1

4. Circuit Simulation

The decoder shown in Fig. 3(a) is constructed by using 230 SET junctions and 289 capacitors. Circuit simulation to confirm the function of the decoder is carried out with SIMON [11]. Depending on received code element c_k, "1"(an electron) or "0"(nothing) is applied to one of the decoder inputs for 40nsec. The input to DL_2 and the output are shown in Fig. 5. Figure 5(a) and (b) show the operation of the decoder when $C = S^0$ and S^1 are received, respectively. From the figures, we confirmed the intended function of the decoder. Figure 5(c) and (d) show that the decoder judges that the received code is $C = S^0$ even if one or two code elements in S^0 are reversed.

The decoder shown in Fig. 3(b) is built of 672 SET junctions and 889 capacitors. Inputs to the four DLs and output of LTG^j are shown in Fig. 6(a), (b), (c), and (d) when $C = S^j$, $j = 0$, 1, 2, and 3, respectively. In addition, we confirmed that LTG^j judges the received code to be S^j when an error is caused on one code element c_k of $C = S^j$, which is not shown in the figure.

5. Conclusions

We have designed SET decoder circuits for THz receivers which consist of a detector based on photoelectric effect and a frequency discriminator based on electron-wave coupling or electron-wave refraction. Results of circuit simulation have validated that the designed decoders function as intended.

Acknowledgment

This work was supported by JSPS KAKENHI Grant No. 15K06075.

References

[1] Y. Tonouchi, Ed., *New Tera-hertz wave Industry*, CMC Press, 2011 (in Japanese).

[2] Y. Kawabata, H. Fujisaka, and T. Kamio, "Probabilistic Particle Modeling of Quantum Wave Propagation with Excitation and Refraction," *Proc. of IEEE ISCAS*, pp.474-477, 2014.

[3] N. Hirami, H. Fujisaka, and T. Kamio, "Probabilistic Particle Modeling of Quantum Wave Propagation with Reflection,

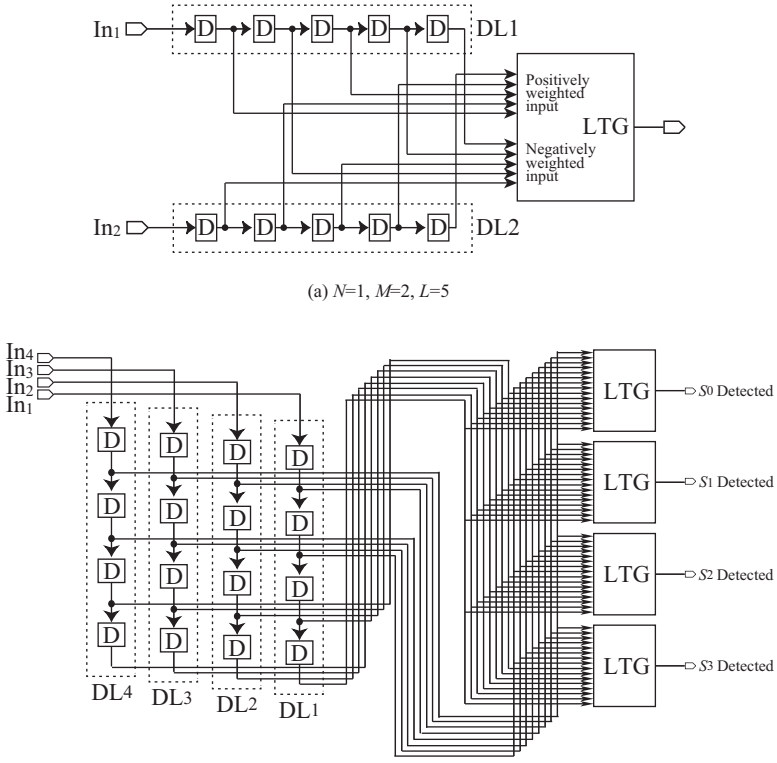

(a) N=1, M=2, L=5

(b) N=2, M=4, L=4

Figure 3: A decoder which consists of DLs and LTGs.

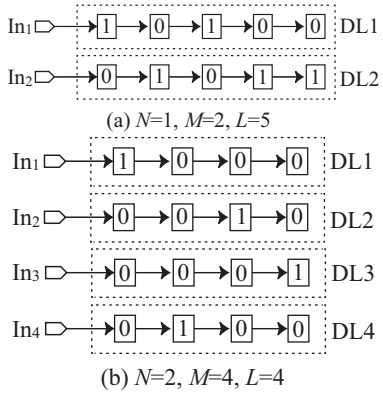

(a) N=1, M=2, L=5

(b) N=2, M=4, L=4

Figure 4: Contents of DLs.

Transmission, and Coupling," *Proc. of IEEE ISCAS*, pp.478-481, 2014.

[4] A. Setsuie, H. Fujisaka, and T. Kamio, "Modeling and Functional Estimation of Coupled Quantum Wave Guide Frequency Discriminator for Spread-Spectrum Frequency Shift Keying Communication," *Proc. of NOLTA*, pp.950-953, 2015.

[5] S. Hamada, H. Fujisaka, and T. Kamio, "Modeling and Functional Estimation of Quantum Wave Lens Frequency Discriminator for Multi-Frequency-Shift Keying Spread Spectrum Communication," *Proc. of NOLTA*, pp.954-957, 2015.

[6] H. Grabert and M. H. Devoret, Eds., *Single Charge Tunneling: Coulomb Blockade Phenomena in Nanostructures*, Plenum Press, 1992.

[7] A. Setsuie, Jinya Sato, H. Fujisaka, and T. Kamio, "Single-Electron Decoder Circuits for Communication Systems Using Photoelectric Effect and Electron Wave Frequency Discrimination," *IEICE Technical Reports*, NLP2016-96, pp.67-72, 2016.

[8] M. W. Keller, J. M. Martinis, N. M. Zimmerman, and A. H. Steinbach, "Accuracy of electron counting using a 7-junction electron pump," *Appl. Phys. Lett.*, Vol. 69, pp.1804-1806, 1996.

[9] C. Lageweg, S. Cotofana, and S. Vassiliadis, "A linear threshold gate implementation in single-electron technology," *Proc. IEEE Comput. Soc. VLSI Workshop*, 2001, pp.93-98.

[10] J. R. Tucker, "Complementary digital logic based on the coulomb blockade," *J. Appl. Phys.*, Vol. 72, No. 9, pp.4399-4413, 1992.

[11] C. Wasshuber, H. Kosina, and S. Selberherr, "SIMON – a simulator for single-electron tunnel devices and circuits," *IEEE Trans. Comput. Aided Design Integr. Circuits Syst.*, Vol. 16, No. 9, pp.937-944, 1997.

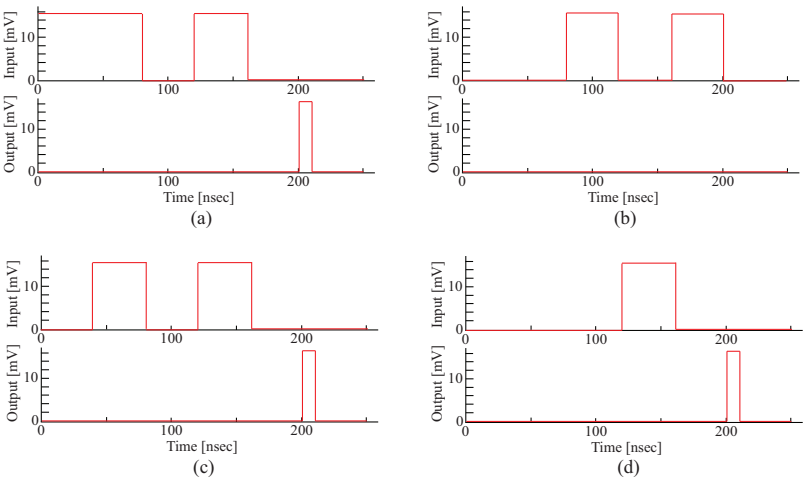

Figure 5: Inputs to the DLs and output of LTG^j.

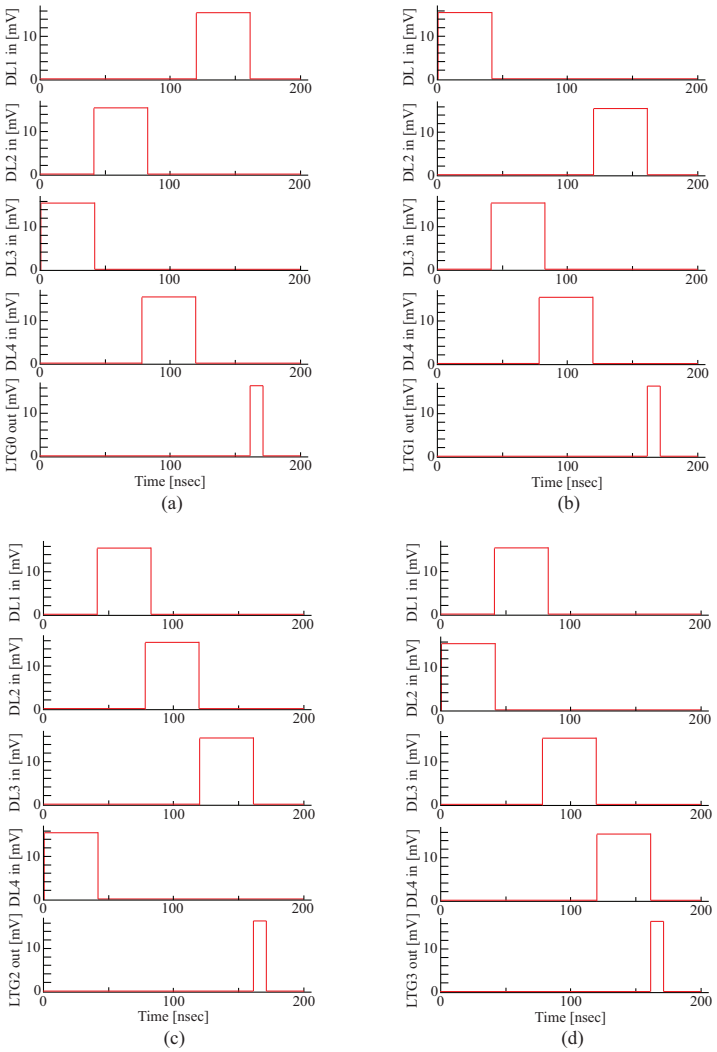

Figure 6: Inputs to the DLs and output of LTG^j.